Available online at www.sciencedirect.com
ScienceDirect
Annals of Nuclear Energy 35 (2008) 1550–1563
annals of NUCLEAR ENERGY
www.elsevier.com/locate/anucene

Transient and stability analysis of a BWR core with thorium–uranium fuel

Alejandro Núñez-Carrera [a], Gilberto Espinosa-Paredes [b,*], Juan-Luis François [c]

[a] *Comisión Nacional de Seguridad Nuclear y Salvaguardias, Dr. Barragán 779 Col. Narvarte, 03020 México, DF, Mexico*
[b] *División de Ciencias Básicas e Ingeniería, Universidad Autónoma Metropolitana, Av. San Rafael Atlixco 186, Col. Vicentina, 09340 México, DF, Mexico*
[c] *Departamento de Sistemas Energéticos, Facultad de Ingeniería, Universidad Nacional Autónoma de México, Paseo Cuauhnáhuac 8532, 62550 Jiutepec Mor., Mexico*

Received 4 December 2007; received in revised form 5 January 2008; accepted 7 January 2008
Available online 4 March 2008

Abstract

The kinetic response of a boiling water reactor (BWR) equilibrium core using thorium as a nuclear material, in an integrated blanket–seed assembly, is presented in this work. Additionally an in-house code was developed to evaluate this core under steady state and transient conditions including a stability analysis. The code has two modules: (a) the time domain module for transient analysis and (b) the frequency domain module for stability analysis. The thermal–hydraulic process is modeled by a set of five equations, considering no homogeneous flow with drift-flux approximation and non-equilibrium thermodynamic. The neutronic process is calculated with a point kinetics model. Typical BWR reactivity effects are considered: void fraction, fuel temperature, moderator temperature and control rod density. Collapsed parameters were included in the code to represent the core using an average fuel channel. For the stability analysis, in the frequency domain, the transfer function is determined by applying Laplace-transforming to the calculated pressure drop perturbations in each of the considered regions where a constant total pressure drop was considered. The transfer function was used to study the system response in the frequency domain when an inlet flow perturbation is applied. The results show that the neutronic behavior of the core with thorium uranium fuel is similar to a UO_2 core, even during transient conditions. The stability and transient analysis show that the thorium–uranium fuel can be operated safely in current BWRs.

1. Introduction

The use of thorium in light water reactors has several potential advantages over the uranium–plutonium cycles in commercial nuclear power plants. First, thorium is a more abundant resource than uranium and second, the thorium cycle has the capability to improve the fuel conversion in a once-through cycle in thermal reactors. Other important point is that the thorium cycle tends to reduce the proliferation of spent fuel, this is much more favorable because it reduces the plutonium production and the decay heat amount. Finally, the thorium cycle reduces the long-lived minor actinides production compared with the uranium and plutonium cycle; and the radiotoxicity level of spent fuel is less in the thorium cycle than the others, in the case of the once-through cycle in light water reactors (LWR). Due to this characteristic and the increasing demand of clean electricity, many research institutes have projects related with the thorium nuclear fuel cycle.

The work of Todosow et al. (2005), summarizes some of the results of recent studies of the performance of thorium-based fuels in LWRs. It concludes that the use of heterogeneous U–Th fuel provides higher neutronic potential than a homogeneous fuel. The U–Th fuel can yield reduced spend-fuel volume, toxicity and decay heat. Additionally, the mix of Pu–Th increases the burnup of Pu.

An equilibrium fuel cycle for a pressurized water reactor (PWR) loaded with an homogeneous mixture of uranium–thorium (ThO_2–UO_2) was studied by Saglam et al. (2005),

* Corresponding author. Fax: +52 55 5804 4900.
E-mail address: gepe@xanum.uam.mx (G. Espinosa-Paredes).

0306-4549/$ - see front matter © 2008 Elsevier Ltd. All rights reserved.
doi:10.1016/j.anucene.2008.01.007

their results indicated that the design is technically feasible in modern PWRs, however there is an additional cost associated with the use of this kind of nuclear fuel. The use of weapons-grade plutonium in PWR fuel assembly was studied by Dzjadosz et al. (2005). This work examined the core safety parameters for a LWR. The analysis of selected transient showed the feasibility of licensing thorium mixture fuel, becasuse it has less severe consequences than a core with low enrichment uranium fuel. Previously, Macdonald and Lee (2004) studied the neutronic, economic and mechanical behavior of the thorium–uranium dioxide fuel in light water reactors, under normal operation and accident conditions. One of the main results is that the thorium–uranium spent fuel is much more stable waste form than uranium oxide spent fuel. Shwageraus et al. (2004) studied the spatial separation of the uranium and thorium parts of the fuel to improve the achievable burn-up of the thorium–uranium fuel, through more effective breeding of U-233 from Th-232, however the large power imbalance between the uranium and the thorium regions creates several design challenges. Joo et al. (2004) showed alternative applications of homogeneous thoria–urania fuel in PWR. Their study shows that the neutronic behavior of a mixed thorium and uranium dioxide $(Th + U)O_2$, is not significantly different from the UO_2 core. This means that homogeneous thorium–uranium fuel can be used without any important mechanical modification of the fuel and design limits. Núñez-Carrera et al. (2005) proposed a design of thorium–uranium fuel using the blanket–seed concept. They showed that the main operational parameters of a thorium–uranium core are similar to that of a standard BWR with uranium fuel, and the economic analysis shows that the fuel cost can be competitive with the cost of a standard uranium core (Núñez-Carrera et al., 2008).

In this work, the study of some typical transients and stability analysis of a BWR, using the thorium–uranium fuel designed by Núñez-Carrera et al. (2005), is presented. The first part of this paper briefly describes the thorium–uranium fuel and the model used to evaluate the core behavior during transient conditions. The last part of the paper shows the results of the simulation of three transients and the stability analysis. These results show that the proposed fuel design can work safely, and can be easily implemented in current BWRs, but this could be take a long time because the actual technology of the BWR is based in the uses of the traditional uranium enrichment fuel.

2. Fuel design

The objective of this work is to study the dynamic response of the core of a typical BWR using the thorium–uranium fuel and to show the safety operation of this core under transient conditions. The design and analysis of the thorium–uranium fuel was performed using the lattice physics code HELIOS (Studsvik Scandpower, 1998), which was previously validated for thorium applications in LWRs by Núñez-Carrera et al. (2004). An in-house code was developed to perform the stability and transient analysis. The description of the models and the performance of this code are presented in the work of Espinosa-Paredes et al. (2006).

The thorium–uranium fuel is designed under the integrated blanket–seed concept (Núñez-Carrera et al., 2005), it means that the blanket and the seed rods are together located in the same fuel assembly and are burned-out in a once-through cycle to improve the conversion capability, in order to have sufficient control reactivity and to obtain negative Doppler and void reactivity coefficients. The blanket–seed concept was adopted and a triangular pitch lattice was designed. This design includes the blanket sub-lattice (ThO_2 rods, located in the corners) and the seed sub-lattice, with U-235 enriched uranium and designated by U-235/Zr (located in the center), in a heterogeneous arrangement integrated in one standard BWR assembly, as it is shown in Fig. 1. In this concept, blanket regions contain higher fraction of fertile material and the blanket volume is higher than the seed regions volume (Ronen, 1986). The blanket rods have only thorium in the form of ThO_2 and the seed rods are made of metal fuel in the form of U-235 enriched uranium–zirconium alloy (U-235/Zr), as it is proposed by Galperin et al. (1997) and Kim and Woo (2000). The defined triangular blanket–seed lattice is composed by the blanket sub-lattice and the seed sub-lattice. The blanket sub-lattice will be first loaded in the core (one cycle) in order to produce its own fuel (mainly U-233). At this step, the center of the triangular lattice is occupied by a dummy zircaloy rod instead of the seed rod. At the next cycle, the blanket sub-lattice will be assembled with the fresh seed sub-lattice to form the blanket–seed lattice (the dummy zircaloy sub-lattice is retired at this time).

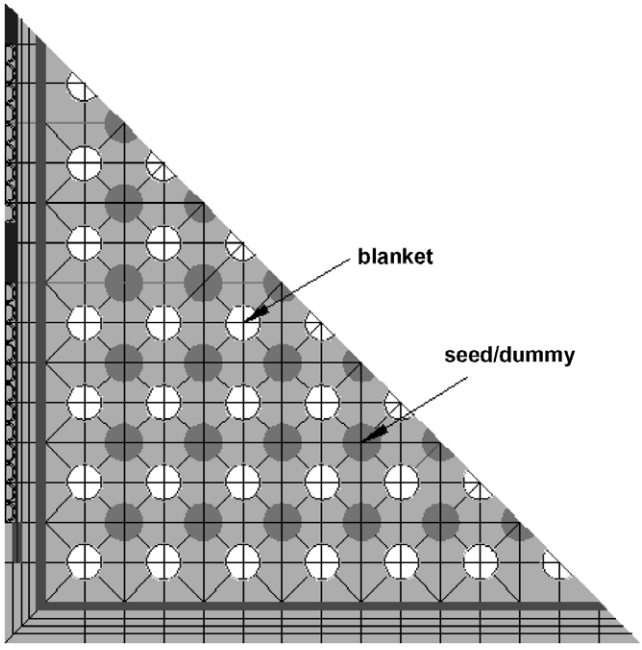

Fig. 1. Integrated blanket (white pin)–seed (dark pin) fuel design.

Table 1
Blanket–seed fuel assembly parameters

Parameter at cold zero power	Blanket–seed/Dummy
Pitch	1.91 cm
Fuel pellet outer radius (blanket)	0.4025 cm
Clad inner radius (blanket)	0.411 cm
Clad outer radius (blanket)	0.4759 cm
Fuel pellet outer radius (seed/dummy)	0.400 cm
Clad inner radius (seed/dummy)	0.400 cm
Clad outer radius (seed/dummy)	0.44 cm
Fuel channel inside dimension	13.4061 cm
Fuel channel wall thickness	0.1651 cm
Density of thorium dioxide	9.424 g/cm^3
Density of uranium–zirconium	16.50 g/cm^3
Zirconium (clad)	6.40 g/cm^3
Thorium mass fraction in the core	0.476
Uranium–zirconium mass fraction in the core	0.469
Zirconium (clad) mass fraction in the core	0.055
Thorium volume fraction in the core	0.576
Uranium–zirconium volume fraction in the core	0.324
Zirconium (clad) volume fraction in the core	0.100

The proposed design has a good reactivity performance with a U-235 enrichment of 5.5%. Regarding the reactivity void coefficient, the proposed uranium–thorium fuel has always a negative value: −240 pcm at beginning of life (BOL) and −54 pcm at a burn up of 60,000 MWd/T. Table 1 shows the main design parameters of the proposed fuel at the cold zero power condition (Núñez-Carrera et al., 2005).

3. Equilibrium core design

The core of Laguna Verde Nuclear Power Plant was chosen as base case for the design of a typical BWR core. This is a small core with 444 fuel assemblies, rated at 2027 MWth; therefore the challenge was to locate the blanket–dummy assemblies and the blanket–seed assemblies in such way to achieve the U-233 breeding while keeping a reasonable power distribution to obtain a desired cycle length. Calculations were performed with CM-PRESTO code (Scandpower, 1992a), which is a three-dimensional neutronic–thermal–hydraulic steady-state code. Nuclear data banks were generated with the HELIOS system and they were processed by TABGEN (Scandpower, 1992b) to produce tables of nuclear cross sections depending on burn-up, void and exposure weighted void (void history) which are used by CM-PRESTO. The Hailing (1963) strategy was used in order to obtain an equilibrium cycle length of 365 effective full power days (EFPD) with an assumed end of cycle target eigenvalue. In a multi-cycle procedure, sufficient number of cycles were run until no changes were observed in cycle length, power, burn-up and void distributions in the core (equilibrium cycle).

4. Model descriptions

The numerical model developed is described with detail in Espinosa-Paredes et al. (2006), and was used to perform transient and linear stability analysis for a boiling water reactor core based on an integrated blanket–seed thorium–uranium concept. This model was based in lumped and distributed parameters approximations, which includes the vessel dome and the downcomer, the recirculation loops, the neutron process, the fuel pin temperature distribution, the core lower and upper plenums and the pressure and level controls. The stability was determined by studying the linearized versions of the equations representing the BWR system in the frequency domain. The thermal–hydraulic model that describes the dynamic behavior of the lower and upper plenums and the reactor core, as well as the fuel temperature model, was based on the distributed parameters approximation. The vessel dome, downcomers, recirculation loops and neutron process models were based on the lumped parameters approximation.

4.1. Thermal–hydraulic model

The thermal–hydraulic model consists in five equations model, which are based on liquid and gas phase mass balances, mixture momentum, mixture energy and liquid phase energy, together with a drift flux approach (Zuber and Findlay, 1965), for the analysis of phase separation. The non-equilibrium two phase flows for the volumetric vapor generation rate in subcooled boiling (Lahey, 1978) was considered using Saha and Zuber (1974) approximation.

A multi-node fuel pin model was developed to describe the heat transfer process. Three regions were identified as minimum to be considered in the heat transfer analysis: The first region corresponds to heat transfer in the fuel; the second region corresponds to heat transfer in the gap and the third region corresponds to heat transfer in the clad, whose temperatures were determined by the rate of heat convection due to the core flow.

The reactor power is calculated from a point reactor kinetics model with six groups of delayed neutrons. The reactivity due to Doppler effect, void fraction, moderator temperature and control rod were considered in this model. In order to complete the study, an analytical procedure with linear analysis in frequency domain is presented to calculate the BWR instability physical parameters.

The recirculation model includes the pressure drops and flows from the downcomer, recirculation pumps, nozzles, jet pumps throat and diffuser, lower and upper plenum, reactor core and steam separators, in order to obtain the momentum balances. The recirculation system flow path is shown in Fig. 2.

Fig. 3 is a schematic diagram of the boiling water reactor where the arrangement of the computational cells of the BWR-5 mode is shown. The reactor vessel was divided into five zones. Two of these zones, the vessel dome and the downcomer, have a variable volume according to the vessel water level. The three fixed volume zones are the lower plenum, which includes the jet pump volume; the upper plenum and the steam separators, and the reactor core. Due to its importance on the model performance, the latter was subdivided

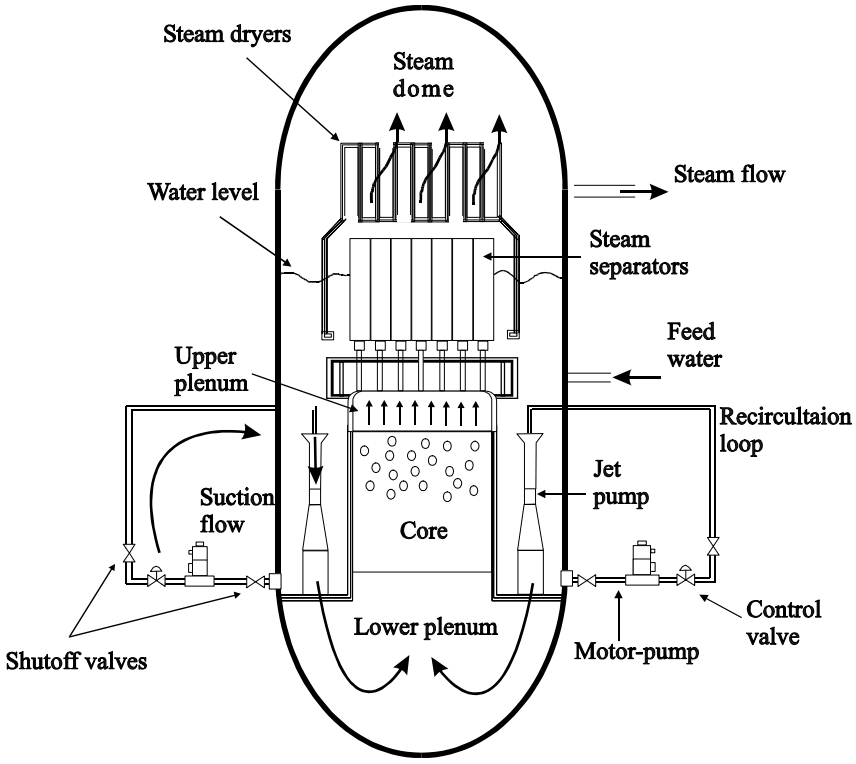

Fig. 2. Recirculation system flow path.

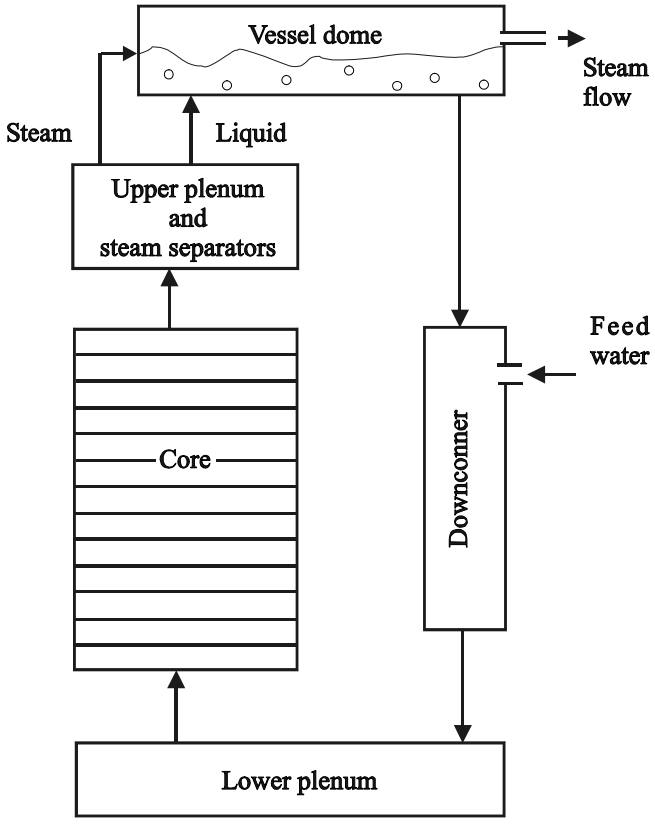

Fig. 3. Arrangements of the computational nodes in the BWR model.

into 12 one-dimensional nodes. The reactor model is completed by including the recirculation loops, the neutron kinetics, the fuel rod temperature and the control models. In addition, this model uses a set of empirical correlations valid for the normal range of BWR operating conditions.

4.2. Stability model using frequency-domain linear analysis

Since secure power generation is the main task in BWR, the understanding of the physical mechanism that induces the observed power oscillation is of paramount importance for BWR operation. In principle, the understanding of such physical mechanisms would lead to improved BWR reactor design, operation strategies and control. The interaction and feedback mechanisms between heat transfer process, thermal–hydraulic (single phase and two-phase flow patterns) and neutronic dynamics in BWRs lead to complex behavior with stationary and no-stationary power oscillation. In the last few decades, research by Lahey and Podowski (1989) and March-Leuba (1990, 1991, 1993), amount many others has been devoted to the study of the nature of power oscillations and the mechanisms that generate them. Several approaches have been taken to address the stability of BWRs, March-Leuba (1986) pioneered the study of reduced-order models for coupled thermal–neutronic dynamics.

In this work, the stability model considers an averaged fuel channel, which was divided into two regions. The first region corresponds to one phase flow and the second region corresponds to two-phase flow. The fuel channel is uniformly heated and the total pressure drop is considered to be constant. The pressure drop in each of the regions is affected as a result of the perturbation influence.

The block diagram of a BWR in liberalized model is shown in Fig. 4. The complicated thermohydraulic transfer functions are collapsed into one transfer function to investigate dynamic stability:

$$G(s) = \frac{1}{1 + H(s)}, \tag{1}$$

here $H(s)$ is the transfer function given by

$$H(s) = \frac{\Pi(s)}{\Gamma(s)}, \tag{2}$$

where $\Pi(s)$ and $\Gamma(s)$ are transfer functions, which are given in Appendix A.

The thermohydraulic system is in the threshold of instability if the denominator of the transfer function $G(s)$ is equal to zero. This means that the operating conditions have to be such that $H(s) = -1$.

If (q''') is the density power that depend on the void fraction, as in a nuclear reactor, and a perturbation is introduced in the reactivity, as a movement of a control rod, two important effects are identified: a variation in the power reactor due to changes in the average void fraction in the fuel channel and changes in the pressure drop. This is shown in Fig. 5.

4.3. Point reactor kinetics model and power generation

The reactor power is given by

$$P(t,z) = n(t)F(z)P_0, \tag{3}$$

where $F(z)$ is the axial power factor, P_0 is nominal power and $n(t)$ is the normalized neutron flux, which is calculated from a point reactor kinetics model with six groups of delayed neutrons:

$$\frac{dn(t)}{dt} = \frac{\rho(t) - \beta}{\Lambda} n(t) + \sum_{i=1}^{6} \lambda_i c_i(t), \tag{4}$$

$$\frac{dc_i(t)}{dt} = \frac{\beta_i}{\Lambda} n(t) + \lambda_i c_i(t), \quad i = 1, 2, \ldots, 6, \tag{5}$$

where c_i is the delayed neutron concentration of the Ith precursor group normalized with the steady-state neutron density, ρ is the net reactivity, β is neutron delay fraction, Λ is the mean prompt neutron generation time, λ_i is the decay constant of the ith delayed neutron precursor, β_i is

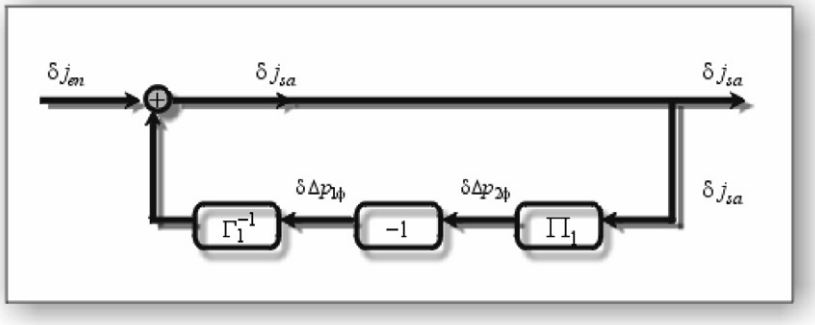

Fig. 4. Block diagram of a BWR in the linearized model. δ is perturvation in variable j_{en}, j_{sa}, $p_{1\phi}$ and $p_{2\phi}$; Γ and Π are transfer functions without feedback.

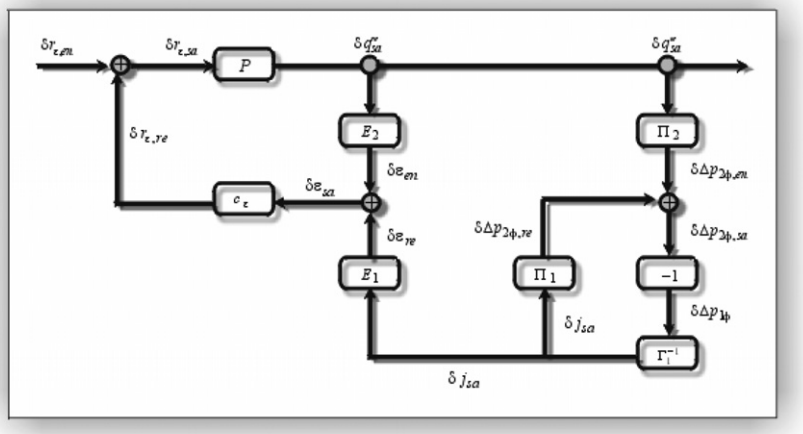

Fig. 5. Block diagram of a BWR in the linearized model. δ is perturvation in variable r_ε, q''_{sa}, $p_{1\phi}$ and $p_{2\phi}$; E, P, Γ and Π are transfer functions with feedback.

the portion of neutrons generated from the ith group precursor. The initial conditions are given by

$$n(0) = n_0, \tag{6}$$

$$c_i(0) = \frac{\beta_i n_0}{\Lambda \lambda_i}. \tag{7}$$

The net reactivity of the nuclear reactor includes four main components: feedback reactivity due to the void fraction in two-phase flow (ρ_v), Doppler effect (ρ_D) due to fuel temperature, moderator temperature (ρ_m) and reactor control rods (ρ_{cr}). Therefore, the total feedback reactivity is written as

$$\rho(t) = \rho_v(\langle \varepsilon_g \rangle) + \rho_D(\langle T_f \rangle) + \rho_m(\langle T_m \rangle) + \rho_{cr}(CRP), \tag{8}$$

where $\langle T_f \rangle$ is the average fuel temperature, $\langle \varepsilon_g \rangle$ is the average void fraction, $\langle T_m \rangle$ is the average moderator temperature and CRP is the control rod position. The volume averaged values are calculated by

$$\langle \psi \rangle = \frac{1}{V} \int \int \int_V \psi \, dV, \tag{9}$$

where ψ is the generic variable.

The point kinetic equations are stiff in the coefficients because they are different in several orders of magnitude, especially in Eq. (4). The variable implicit integration method, as reported in Wulff et al. (1984)), was used to solve Eq. (4), and the Euler method in explicit form was used to solve the delayed precursor concentration given by Eq. (5).

Since the thermal–hydraulic and neutronic model uses an average fuel channel to represent the full core, it was necessary to collapse the main parameters to introduce them into the in-house computer code (Espinosa-Paredes et al., 2006). This collapsing process is described in the following section.

4.4. Collapsing of kinetics parameters

Figs. 6 and 7 show the steady-state radial power and burnup distributions, respectively, for a quarter of core. These values were obtained with CM-PRESTO (Scandpower, 1992a) for an equilibrium core (Núñez-Carrera et al., 2005).

22	22	22	23	22	20	14				
97	96	99	101	101	94	80	25			
47	92	46	123	49	119	40	85	27		
141	136	106	128	130	134	114	40	85	25	
141	125	130	113	133	123	128	114	40	80	16
132	141	124	134	139	140	123	135	120	94	19
144	129	138	124	117	139	133	130	49	101	23
129	141	129	126	124	134	113	128	124	102	24
126	128	127	130	138	124	130	106	46	99	22
122	124	128	141	129	141	125	136	92	96	22
120	122	126	129	144	132	141	141	48	97	22

Fig. 6. Relative radial power × 100 for a quarter of core loaded with blanket–seed fuel.

0	0	0	0	0	0	0				
0	0	0	0	0	0	0	0			
0	365	0	0	0	0	0	0	0		
0	0	351	79	97	0	119	0	0	0	
101	260	135	359	134	241	85	119	0	0	0
234	94	274	141	100	85	242	0	0	0	0
98	266	123	265	341	100	134	97	0	0	0
241	96	225	236	265	141	356	80	0	0	0
226	207	233	212	123	274	135	352	0	0	0
239	233	207	96	266	94	260	0	365	0	0
236	239	226	242	99	235	101	0	0	0	0

Fig. 7. Burnup (MWd/T)/100 for a quarter of core loaded with blanket–seed fuel.

The main parameters of the numerical point kinetics model per neutronic channel are the neutron delay fraction, the mean prompt neutron generation time, the decay constant of the delayed neutron precursor and the portion of neutrons generated from the ith group precursor. For the collapsing of these values used in Eqs. 4, 6 and 7, a numerical regression was used to fit these values under the following criterion:

- The delayed neutrons fraction, β, was fitted using a linear regression as a function of burnup.
- The final kinetic parameters collapsing were obtained using the neutron flux as weight function according with the following expressions:
  a) The delayed neutrons fraction is calculated using the neutron flux ϕ_i per node as follows:

$$\beta = \frac{\sum_i \beta_i \phi_i}{\sum_i \phi_i}. \tag{10}$$

  b) The neutron generation time (Λ) for the whole core is calculated using the following expression:

$$\Lambda = \frac{1}{(\Sigma_{a1} + D_1 B_1^2 + \Sigma_{a2} + D_2 B_2^2)v}, \tag{11}$$

  where v is the velocity of the neutrons, Σ_a is the absorption macroscopic cross-section, D is the diffusion coefficient and B is the geometric buckling for the fast group (subindex 1) and thermal group (subindex 2). These parameters where obtained from PETRA (Scandpower, 1992c) computer code. The averaging schemes in PETRA are based on the principle of preserving reactivity effects by importance weighting of diffusion equation parameters. Kappa–sigma fission is collapsed by PETRA by simple volume weighting in order to preserve the axial power shape. Table 2 shows a comparison between the typical values of the delay neutrons fraction for UO_2 fuel and those obtained for the blanket seed thorium fuel. The values of this table for UO_2 correspond to the beginning of cycle (BOC) and were taken from the final safety analysis report (FSAR) of a typical BWR-5 (Comisión Federal de Electricidad, 1979).

Table 2 shows that the total delayed neutron fraction β for the blanket–seed fuel is about 10% higher than that of the UO_2 fuel. U-233 has a delayed neutron fraction lower than U-235, and for thorium, it is about one order of magnitude higher than U-235; being therefore is the most dominant. A higher delayed neutron fraction causes that the period of the reactor be higher and therefore improves the control of the neutronic population.

Table 2 shows the λ_i values used for U-235 and Th-232. This table shows that the decay constant for these fuels are very similar. Therefore, Table 2 shows that the kinetics behavior of both fuels is almost the same.

4.5. Collapsing of geometric parameters

The next step was the collapsing of geometric parameters for the calculation of thermal–hydraulic properties of the fluid. These properties are evaluated in the center of the core and we assume that the coolant is uniformly distributed. Two types of fuel assemblies were considered: blanked-seed and blanket dummy. These were defined using the unitary cell. Using this cell, we define parameters as well as cross-sectional area of the channel (wet perimeter), heated perimeter, hydraulic diameter and heat transfer area.

The geometrical dimension of the blanket, seed and dummy pins are almost the same. Table 3 shows these dimensions. The model considered only one hydraulic channel divided in 12 hydraulics nodes.

All the geometrical parameters were referenced respect to unitary cell. We considered that the core of the reactor has 444 fuel assemblies. Each fuel assembly has 49 unit cells. Under this consideration we obtain the following parameters.

The equivalent hydraulic diameter is defined by

$$D_h = \frac{4A_{x-s}}{Z}, \tag{12}$$

Table 3
Main parameter in the design of the fuel pin

Symbol	Description	Value
$D_c = D_{c_e} - E_c$	Inner diameter of the clad	0.00822 m
D_{c_e}	External diameter of the clad	0.009518 m
P	Pitch	0.0180 m
D_f	Diameter of the fuel pellet	8.050×10^{-3} m
L_b	Length of the fuel, bar	3.81 m
L_n	Length of the node	0.3175 m
E_c	Thickness of the clad	6.49×10^{-4} m

Table 2
Kinetics parameter values for the blanket–seed fuels UO_2 fuels

Delay neutron fraction	Blanket–seed	UO_2	Decay constant (s^{-1})	Blanket–seed	UO_2
β_1	2.72×10^{-4}	2.47×10^{-4}	λ_1	0.0130	0.0127
β_2	1.26×10^{-3}	1.38×10^{-3}	λ_2	0.0321	0.0317
β_3	1.20×10^{-3}	1.22×10^{-3}	λ_3	0.13	0.12
β_4	2.86×10^{-3}	2.65×10^{-3}	λ_4	0.35	0.31
β_5	1.21×10^{-3}	8.32×10^{-4}	λ_5	1.40	1.40
β_6	4.55×10^{-4}	1.69×10^{-4}	λ_6	3.96	3.87
β	7.16×10^{-3}	6.50×10^{-3}			

Table 4
Parameters of blanket–seed and UO_2 fuels

Description	Blanket–seed	UO_2
Flow area per assembly	176.7 cm^2	190.3 cm^2
Hydraulic diameter	1.26 cm	1.52 cm
Heat transfer area	429.95 m^2	328.56 m^2
Total flow area	78460.24 cm^2	84483.53 cm^2
Fuel mass	7.31 tons	8.93 tons
Clad mass	2.34 tons	3.07 tons

Table 5
Total volume fraction of the materials in the reactor with blanket–seed fuel

Material	Volume fraction
Blanket (thorium)	0.58
UZr (dummy–seed)	0.32
Zirconium (clad)	0.10

where A_{x-s} is the flow area and Z is the wetted perimeter of the flow, which are given by

$$A_{x-s} = P^2 - 2 * \left(\frac{\pi}{4}\right) D_{ce}^2 \quad (13)$$

$$Z = \pi D_{ce}, \quad (14)$$

respectively. In these equations, P is the pitch and D_{ce} is the diameter of the fuel element.

The volume of the node in the core is given by

$$V_a = A_{x-s} L_n, \quad (15)$$

where L_n is the node length.

The fuel assembly of Fig. 1 is an array of 7×7 pins of blanket and 6×6 pins of seed (or dummy), i.e., 85 pins per fuel assembly. The core of the reactor has 444 fuel assemblies, 104 are located in the external part of the core and correspond to the blanket–dummy fuel elements. Each fuel element has 85 rods per assembly, therefore, there are 3774 pins of zirconium (dummy). These pins were not considered in the total heat transfer area because they do not produce heat. According to this, the number of active pins elements in the core is 33,996. The total cross-sectional D_H is obtained by multiplying of the hydraulic diameter (D_h) by the number of active pins:

$$D_H = 33996 D_h. \quad (16)$$

The heat transfer area is obtained using the following equation:

$$A_{HT} = \pi D_H L_n. \quad (17)$$

The results of these parameters are shown in Tables 4 and 5.

5. Simulations

An in-house code was developed to evaluate the thorium equilibrium core under steady-state and transient conditions; also a stability analysis was performed. The code has two modules: (a) the time domain module for transient analysis and (b) the frequency domain module for stability analysis. Thermal–hydraulic effects are modeled by a set of five equations (Espinosa-Paredes et al., 2006). The neutronic phenomena are calculated with a point kinetics model. Typical BWR reactivity effects are considered: void fraction, fuel temperature, moderator temperature and control rod density. Collapsed parameters were included in the code to represent the core with an average fuel channel. For the stability analysis, in the frequency domain, the model of Lahey and Podowski (1989) was used, where the system transfer function is determined by applying Laplace-transforming to the calculated pressure drop perturbations in each of the considered regions; the assumption of a constant total pressure drop was applied. The transfer function was used to study the system response in the frequency domain when an inlet flow perturbation is applied.

5.1. Transient analysis

The nominal values used in the transient simulations, presented in this section, correspond to Laguna Verde nuclear power plant, which is a typical BWR-5. The analysis of the events assumes normal functioning of the plant's instrumentation and controls, plant protection and reactor protection systems.

5.1.1. Closure of all main steam line isolation valves

The main steam isolation valves close in 3 s and the position switches of the valves initiate a reactor scram when the valves are less than 90% open. The closure of these valves inhibits the steam flow to the feedwater turbines terminating the feedwater flow (Fig. 8a). Pressure mitigation of increase is accomplished by initiation of the reactor scram via MSIV position switches, the protection system (Fig. 8b), and the opening of the safety relief valves (SRVs), limiting the system pressure (Fig. 8c). The peak pressure will still remain considerably below the ASME code limit of 1375 psig (9.48 MPa) (Fig. 8d). The loss of feedwater flow causes a fast water level decrease, enough (Fig. 8e) to produce the recirculation system trip; this is a protection against cavitations. The starting signal of the emergency core cooling systems (ECCS) system starts at approximately 33 s; however, there is a delay up to 30 s, before the water supply enters the vessel. Nevertheless, there is no change in the thermal margins. The thermal power peak reaches 120% of the rated value after approximately 3 s, due to the drastic reduction of the void fraction in the core.

5.1.2. Simulation of two recirculation pumps trip

In this transient there is a recirculation pump trip, increasing the water level in the reactor vessel due to the reduction of the void fraction. The analysis assumed a pump inertia time constant of 3.0 s, this value was found during the plant startup testing for Laguna Verde nuclear power plant (CNLV) (Fig. 9a). In this transient, the water lever rises in approximately 3 s, but never peaks over the high setpoint, avoiding the reactor trip, as is shown in

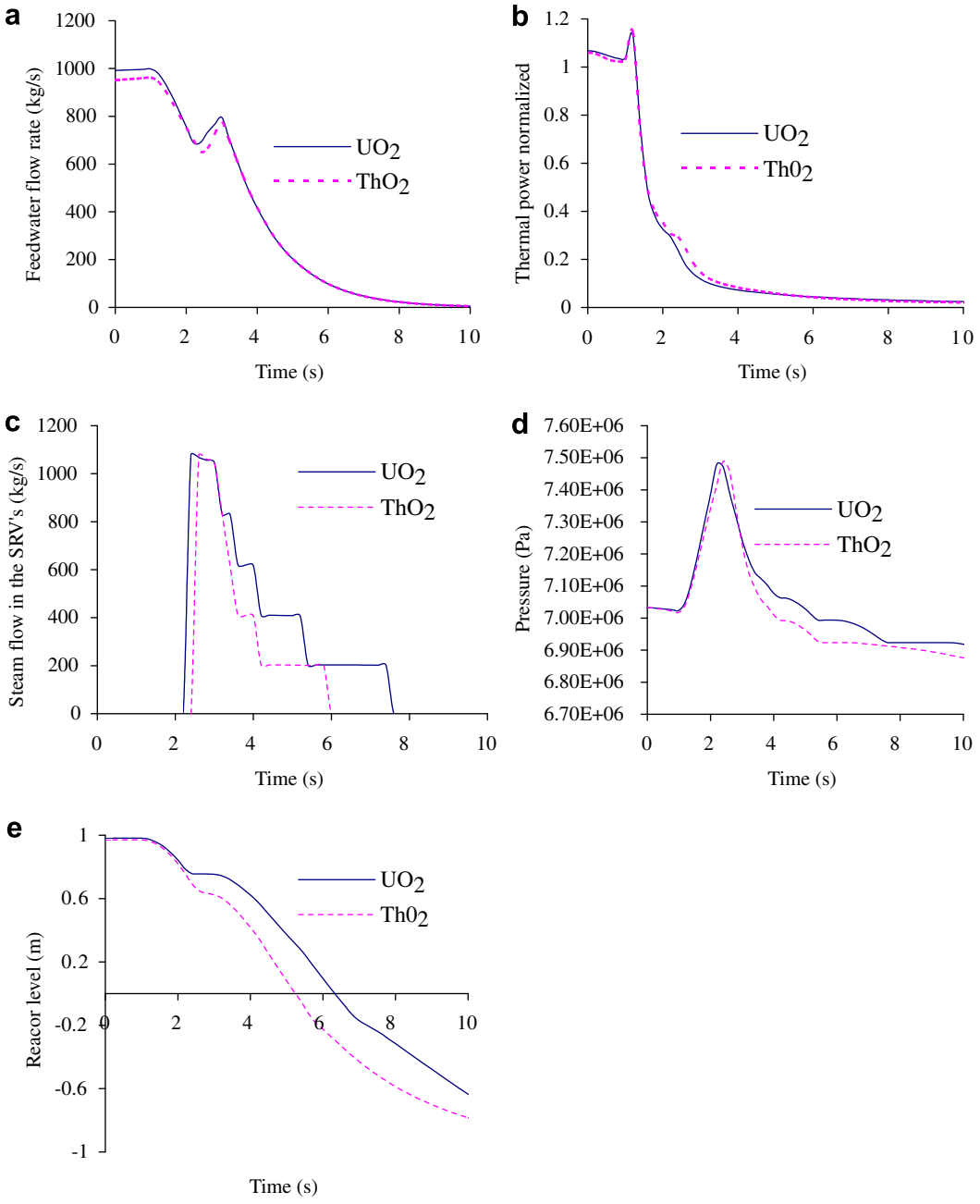

Fig. 8. Closure of all main steam line isolation valves. (a) Feedwater flow during the closure of main steam valves, (b) shutdown of the reactor due to high pressure and high neutron flux during the closure of main steam valves, (c) safety relief valve actuation due to high pressure in the reactor vessel, (d) peak of pressure in the reactor vessel during the closure of main steam valves and (e) reactor level reduction due to the opening of safety relief valves.

Fig. 9b. The increase of the void fraction is shown in Fig. 9c. Since no SCRAM occurs for the trip of two recirculation pumps, no immediate operation action is required. Fig. 9b shows, graphically, that the vessel water level swells due to the rapid flow coastdown, without reaching the high setpoint. The pump trip reduces the core flow and therefore the power decreases to approximately 40% of the rated value (natural circulation), as are shown in Fig. 9d and e, respectively. The core flow reduction involves the reduction of the steam flow and the feedwater due to the actuation of the controllers, as it is shown in Fig. 9f.

The pressure at the dome of the vessel stays very stable due to the action of the control pressure and remains below the 9.48 MPa limit, allowed by the applicable ASME code.

5.1.3. Loss of feedwater flow

In this transient, the feedwater flow terminates at approximately 5 s (Fig. 10a). The loss of fedwater results in a proportional reduction of the water inventory, causing the vessel water level to drop (Fig. 10b). Subcooling decreases causing a reduction in the core power level and the pressure. As the power level is reduced (Fig. 10c), the

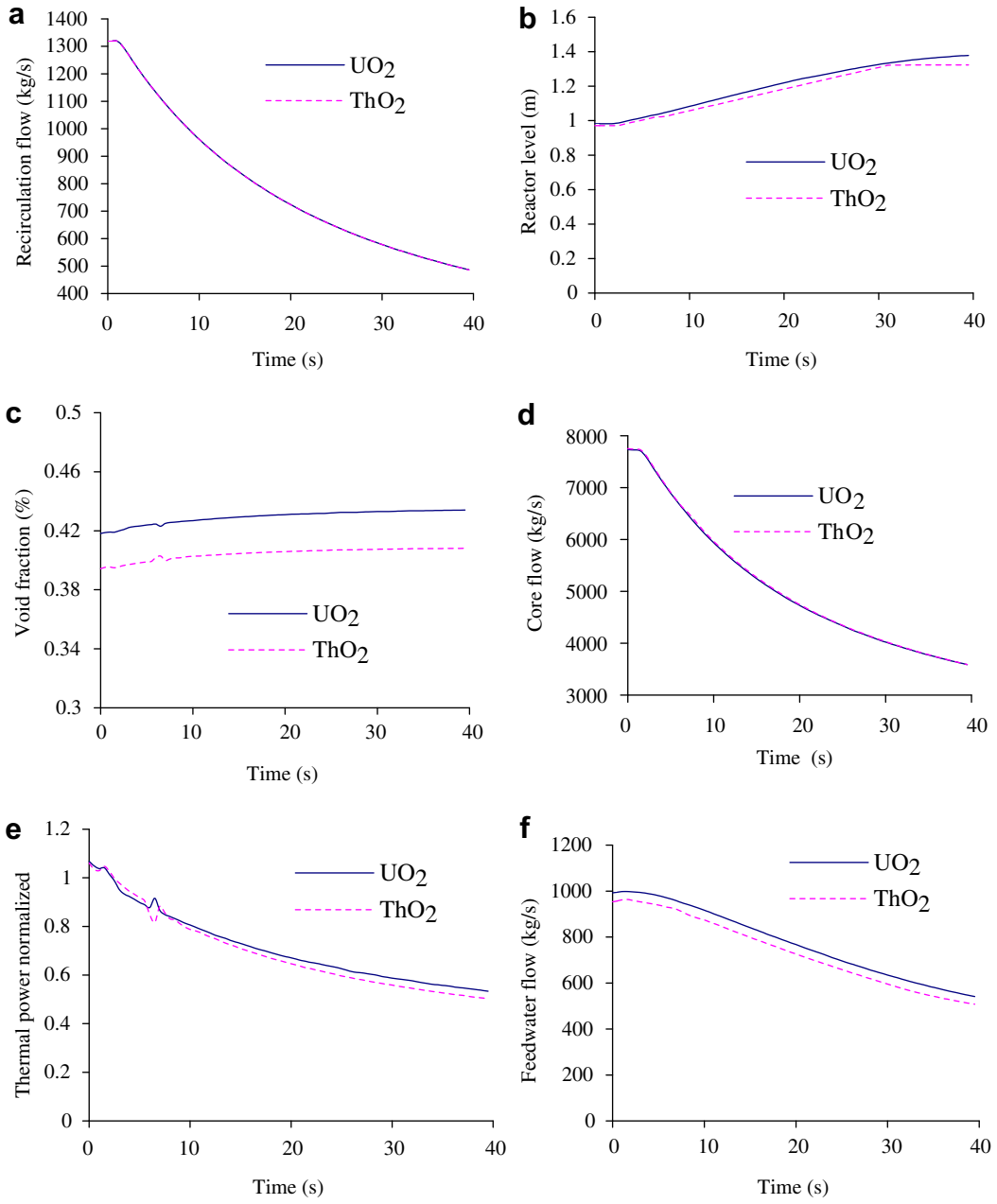

Fig. 9. Recirculation pumps trip. (a) Recirculation flow rate reduction due to trip of pumps, (b) reactor level increases due to reduction of recirculation flow, (c) void fraction increases due to reduction of recirculation flow, (d) core flow reduction after recirculation pump trip, (e) thermal power reduction due to recirculation pump trip and (f) behavior of feedwater, following the steam flow production after recirculation pump trip.

turbine steam flow starts to drop off because the pressure regulator is attempting to maintain the pressure for the first 5 s or so. Water level continues to drop until the scram trip set point of the vessel level is reached (L3), whereupon the reactor is shutdown within 1 s after this trip is activated (Fig. 10c). The main steam line isolation occurs at 19 s because the vessel water drops to the L2 trip. Also at this time, the recirculation system is tripped (Fig. 10d) and the high pressure core spray system (HPCS) and the RCIC operation is initiated.

Operation of the RCIC or HPCS systems is not included in the simulation of the first 25 s of this transient, since the startup of these pumps occurs in the latter part of this time period, and therefore these systems have no significant effects on the results of this transient. The operation of the safety relief valves at 23 s allows the decay heat removal.

5.1.4. SCRAM manual

In the case of a transient with SCRAM, the fast insertion of negative reactivity does not produce significant differences between the case of the ThO_2 and the UO_2 cores in the short term. The main differences occur in the long-term mainly due to the decay heat. On the other hand, the

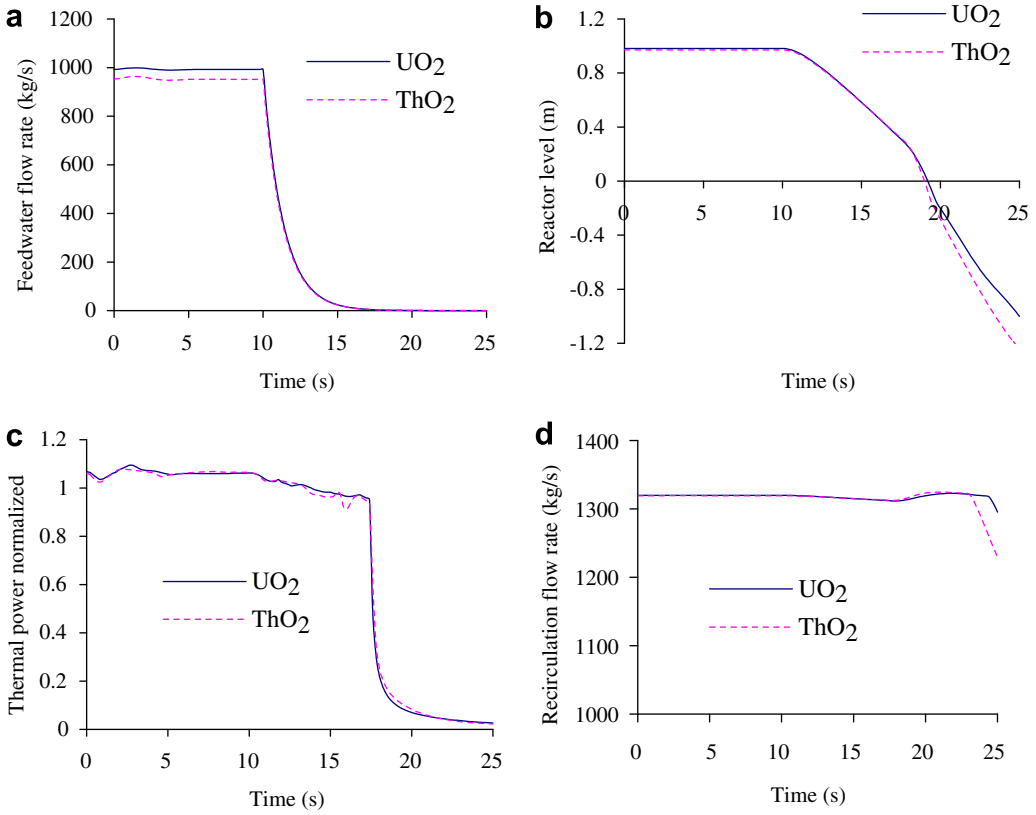

Fig. 10. Loss of feedwater flow. (a) Feedwater behavior after the trip of feedwater pumps, (b) reactor level inventory after the trip of feedwater pumps, (c) reactor shutdown due to low level in the vessel and (d) trip of the recirculation pump due to low level in the reactor vessel.

differences in the loss coefficient due to the different geometrical configuration in the fuels are very important. In the case of the thorium fuel, it is higher, because the pins in the fuel assembly are very tight (see Fig. 1), therefore the pressure drop and the water lever reduction during the transient is higher in the thorium fuel than in the uranium fuel.

5.2. Stability analysis

The operation conditions for the stability analysis can be obtained with previous models in the time domain; using the thermal power and core inlet flow for analysis in the frequency domain.

The instability zone is defined by four points where the system tends to be instable. The borders of this zone are not well established and there are small variations from cycle to cycle. The operational procedures remark the importance to avoid this zone during startups, and operational transients, as the recirculation pump trip.

Five operational states were considered in the study that corresponds to the four corners that define the instability region of the flow–power map, an additional point corresponds to the rated power (100%). Table 6 summarizes the stability results. Analyzing the different values of the boiling length (λ_0) for each state, it can be observed that decreasing the flow through the core, the value of λ_0 decreases, as it was expected. It is known that with a high power–flow relation, the system stability is reduced, this means that λ_0 is a good indicator of the system stability. This is confirmed with the Nyquist diagrams for each state, showed in Fig. 11. The Nyquist stability criteria states that if the close loop function $G(s)$, when plotted on the complex plane, encircles the $-1+0i$ point in a clockwise sense, then the closed loop system will be unstable. According to with this, the operational states number 3 and 5 (Fig. 11c and e) are stable – this result was expected-because they have the lowest values in the power–flow relation and the highest values in the boiling length λ_0. The conclusion is that the most unstable operational state is the number 2 (Fig. 11b) because it posses the highest value in the power–flow relation and the lowest values in the boiling length.

Table 6
Main parameters obtained from the stability analysis

Operational state	Relation P/W[a]	Boiling length λ_0 (m)		Frequency (Hz)	
		Blanket–seed fuel	UO_2 fuel	Blanket–seed fuel	UO_2 fuel
1	1.427	0.884	0.928	0.575	0.377
2	1.739	0.725	0.761	0.590	0.391
3	1.201	1.050	1.103	0.797	0.491
4	1.476	0.854	0.897	0.750	0.487
5	1.050	1.201	1.261	$\gg 1$	1.000

[a] P is the power rate and W is the mass flow in the core.

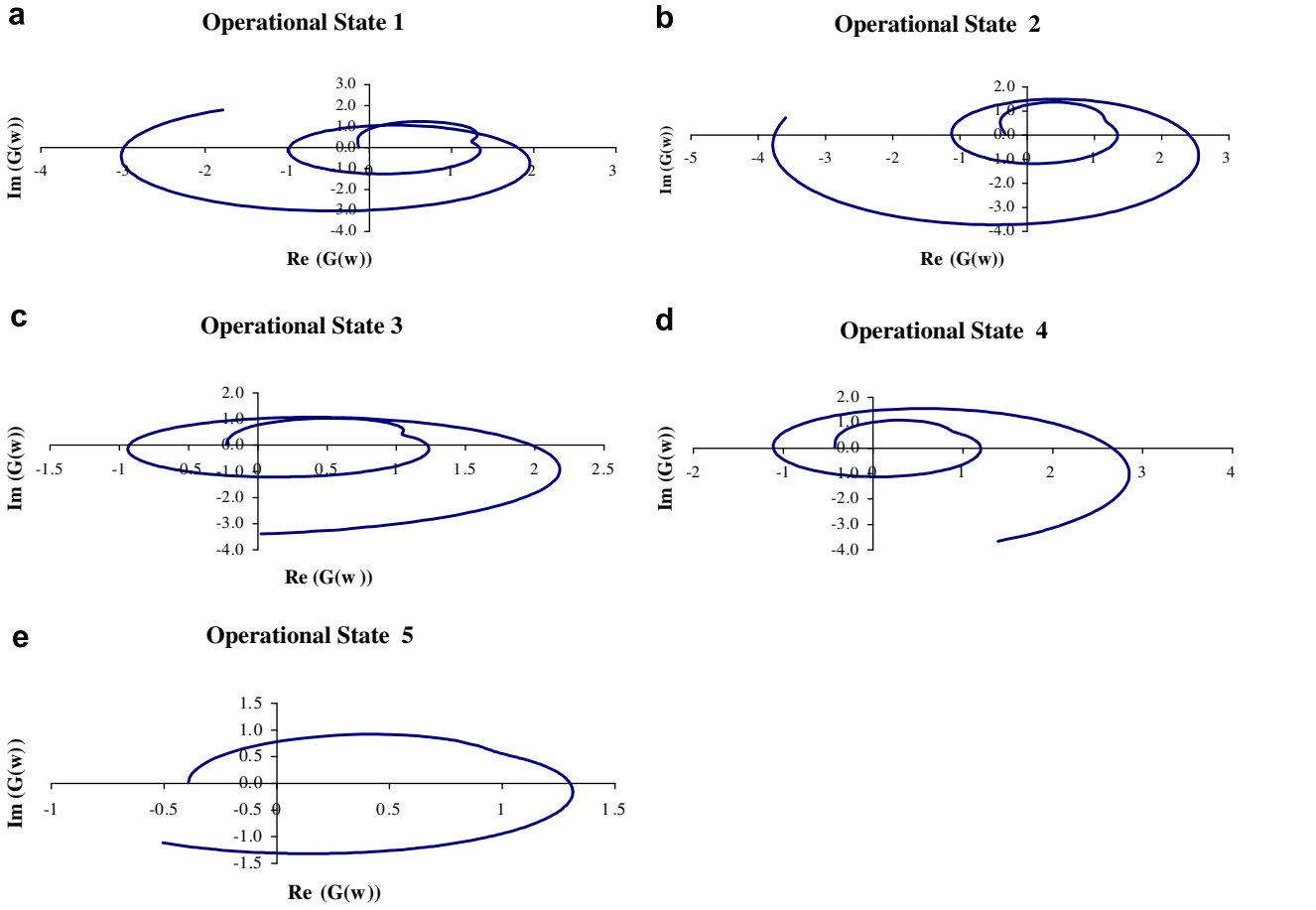

Fig. 11. Nyquist diagram for five operational states. Power flow ratio: (a) 1.359, (b) 1.657, (c) 1.144, (d) 1.406 and (e) 1.0.

The predicted frequency interval value, obtained with this model in the instability regions, goes from 0.377 to 0.49 Hz in the oscillation frequency. While the prediction considering the overall system effects goes from 0.38 to 0.53 Hz, as it is shown in Table 6. This interval is in agreement with that observed with the power oscillation event, because it includes the frequency reported for LVNPP, which is about 0.5 Hz (Espinosa-Paredes et al., 2005).

The results obtained with the thorium fuel show that the characteristic frequency is about 0.5 Hz, which is very typical value for a BWR (NEA, 1997; Verdu et al., 2001).

The table shows that the boiling length for the blanket seed fuel is lower than that of the UO_2 fuel. This is and important point, because the pressure drop is higher for the thorium fuel and therefore is more instable whit higher probability to present the density wave oscillation for operational conditions with low core flow and low power. The operational states 1 and 2 (Fig. 11a and b) are more unstable for the blanked-seed fuel, and the operational states 3 and 4 (Fig. 11c and d) are more unstable for the UO_2 fuel. The operational states 3 and 4 are the more important because they are very close to the startup line after the shutdown of the reactor.

Regarding the instability analysis, five operational states were analyzed; four of them define the traditional instability region corner of the power–flow map, and the fifth one is the operational state for the full power condition. The frequency and the boiling length were calculated for each operational state (Table 6). The frequency of the operational states 1, 2, 3 and 4 is similar to that reported by other authors (NEA, 1997; Verdu et al., 2001); these are instable points that occur due to the density wave oscillation phenomena in some nuclear power plants.

6. Conclusions

A core with thorium and uranium fuel was tested using a simplified model for transient and linear stability analysis in BWR. This model was based on the lumped and distributed parameter approximation, which includes the vessel dome and the downcomer, the recirculation loops, the neutron kinetics, the fuel temperature, the lower and upper plenums reactor core, and the pressure and the level controls. Three transients were presented as an example of application: closure of main steam isolation valves, recirculation pump trip and loss of feedwater. The numerical results obtained with the model show that the transient behavior is similar to the results reported by the FSAR for a typical BWR, as it is illustrated in Figs. 8–10.

Additionally, a stability analysis was performed, where five operational states were considered that corresponds to the four corners that define the instability region of the flow–power map. The fifth operational state corresponds to the rated power (100%), which was used to demonstrate that is fully stable. The results obtained, using the model of this work, are congruent with previous BWRs stability analysis, and the main stability parameters, as the frequency, are very similar for the thorium–uranium fuel and the traditional UO_2 fuel. The same behavior has the boiling length, as it is shown in Table 6.

One of the main conclusions of this work is that the thorium fuel is relatively easy to implement in thermal reactors (BWR), without important changes in the safety systems of the nuclear power station (Núñez-Carrera et al., 2008).

Appendix A. The transfer functions $\Gamma(s)$ and $\Pi(s)$ of Eq. (2) for case that is illustrated by Fig. 4, are defined as follows:

$$\Gamma(s) = \rho_f j_{en,0}\left[\frac{s\lambda_0}{j_{en,0}} + f\frac{\lambda_0}{D_H} + K_{en} + \left(\frac{j_{en,0}f}{2D_H} + \frac{g}{j_{en,0}}\right)\Xi(s)\right], \tag{A.1}$$

where ρ_f is the density of saturated liquid, f is factor friction, g is the acceleration of gravity λ is the length boiling, K_{en} inlet core loss coefficient, j_{en} is inlet core superficial velocity, s is Laplace variable. The steady state of the model is denoted subscript "0".

The steady state of length is given by

$$\lambda_0 = \frac{\rho_f j_{en,0}\Delta h_{sub,0}}{q_0'' P_H}, \tag{A.2}$$

where $\Delta h_{sub,0}$ is the subcooling, q_0'' is the heat flux, P_H is the heater perimeter. The auxiliary variable $\Xi(s)$ is given by

$$\Xi(s) = \frac{\lambda_0}{\Delta h_{sub}}\frac{\varphi_1(s)}{\varphi_2(s)}[1 - e^{-\varphi_1(s)}]. \tag{A.3}$$

Here

$$\varphi_1(s) = \frac{s}{j_{en,0}} - \frac{H_{1\phi,0}P_H}{\rho_f j_{en,0}A_{x-s}Cp_f[1 - H_{1\phi}Z(s)]}, \tag{A.4}$$

$$\varphi_2 = \frac{q_0'' P_H}{\rho_f j_{en,0}A_{x-s}}\left[\frac{0.8}{1 - H_{1\phi,0}Z(s)} - 1\right], \tag{A.5}$$

where $H_{1\phi,0}$ is the heat transfer coefficient and $Z(s)$ is defined by

$$Z(s) = \frac{A_H}{s\langle\rho Cp\rangle_c V_c}, \tag{A.6}$$

where A_H is the heat transfer area and V_c is the fuel volume.

$$\Pi(s) = \rho_f j_{en,0}[F_1(s) - F_2(s)\Xi(s)]. \tag{A.7}$$

The auxiliary variables $F_1(s)$ and $F_2(s)$ are defined as

$$\begin{aligned} F_1(s) = {} & \frac{f(L_c - \lambda_0)(2s - \Omega_0)}{2D_H(s - \Omega_0)} - \frac{j_{en,0}f}{2D_H}\frac{\Omega_0}{(s - \Omega_0)(s - 2\Omega_0)} \\ & \times [1 - e^{-(s-2\Omega_0)\tau_{LC}}] + \frac{s^2\tau_{LC}}{(s - \Omega_0)} + \frac{g}{j_{en,0}}\frac{1}{(s - \Omega_0)} \\ & \times \left[1 - e^{-\Omega_0\tau_{LC}} - \frac{\Omega_0}{s}(1 - e^{-s\tau_{LC}})\right] \\ & - \frac{\Omega_0^2}{(s - \Omega_0)^2}[1 - e^{-(s-\Omega_0)\tau_{LC}}] \\ & + K_{sa}\left\{1 + \frac{\Omega_0}{2(s - \Omega_0)}[1 - e^{-(s-\Omega_0)\tau_{LC}}]\right\}, \end{aligned} \tag{A.8}$$

$$\begin{aligned} F_2(s) = {} & \frac{\Omega_0 s^2\tau_{LC}}{(s - \Omega_0)} + \frac{f(L_C - \lambda_0)}{2D_H}\frac{\Omega_0(2s - \Omega_0)}{(s - \Omega_0)} \\ & - \frac{\Omega_0^2 s}{(s - \Omega_0)^2}[1 - e^{-(s-\Omega_0)\tau_{LC}}] \\ & - \frac{j_{en,0}}{2D_h}\frac{\Omega_0 s}{(s - \Omega_0)(s - 2\Omega_0)}[1 - e^{-(s-\Omega_0)\tau_{LC}}] \\ & + \frac{g}{j_{en,0}}\frac{\Omega_0}{(s - \Omega_0)}[e^{-s\tau_{LC}} - e^{-\Omega_0\tau_{LC}}] + \Omega_0 + \frac{j_{en,0}f}{2D_h} + \frac{g}{j_{en,0}} \\ & - K_{sa}\Omega_0\left\{\frac{1}{2}e^{s\Omega_0\tau_{LC}} - 1 - \frac{\Omega_0}{2(s - \Omega_0)}[1 - e^{-(s-\Omega_0)\tau_{LC}}]\right\}, \end{aligned} \tag{A.9}$$

where L_C is the core length, τ_{LC} is the time constant and K_{sa} is the outlet core loss coefficient. Finally

$$\Omega_0 = \frac{q_0'' P_H}{A_{x-s}}\frac{\upsilon_{fg}}{h_{fg}}, \tag{A.10}$$

$$\tau_{LC} = \frac{1}{\Omega_0}\ln\left[\frac{j_0(L_C)}{j_{en,0}}\right]. \tag{A.11}$$

In these equations, υ_{fg} and h_{fg} are the difference of specific volumes ($\upsilon_g - \upsilon_f$) and latent heat of vaporization ($=h_g - h_f$), respectively.

References

Comisión Federal de Electricidad, 1979. Final safety analysis report, Central Laguna Verde Unit 1, México, DF, Mexico.

Dzjadosz, D., Ake, T., Saglam, M., 2005. Weapons-grade plutonium–thorium PWR assembly design and core safety analysis. Nuclear Technology 147, 69–83.

Espinosa-Paredes, E., Núñez-Carrera, A., Vázquez-Rodríguez, A., 2006. Simplified distributed parameters BWR Dynamic Model for transient and stability analysis. Annals of Nuclear Energy 33, 1245–1259.

Espinosa-Paredes, G., Prieto-Guerrero, A., Nuñez-Carrera, A., Amadaor-García, A., 2005. Wavelet-based method for instability analysis in boiling water reactor. Nuclear Technology 151, 250–260.

Galperin, A., Reichert, P., Radkowsky, A., 1997. A thorium fuel cycle for light water reactor reducing proliferation potential of nuclear power fuel cycle. Science & Global Security 6, 265–290.

Hailing, R.K., 1963. Operating strategy for maintaining an optimum power distribution throughout life. ANS topical meeting on nuclear performance of power reactor cores. TID 7672.

Joo, K.K., Noh, J.E., Yoo, J.W., Cho, J.Y., Park, S.Y., Chang, M.H., 2004. Alternative applications of homogeneous thoria–urania fuel in

light water reactors to enhance the economics of the thorium fuel cycle. Nuclear Technology, 37–52.

Kim, M.-H., Woo, I.-T., 2000. Once-through thorium fuel cycle options for the advanced PWR core. In: ANS Proc. Int. Topl. Mtg. Reactor Physics, Mathematics and Computation and Nuclear Criticality Safety (Physor 2000), Pittsburgh, PA.

Lahey, R.T., 1978. A mechanistic subcooled boiling model. In: Proc. of Sixth Int. Heat Transfer Conf.

Lahey, R.T., Podowski, 1989. On the analysis of various instabilities in two-phase flow. In: Hewitt, G.F., Delhaye, J.M., Zuber, N. (Eds.), Multiphase Science and Technology. Hemisphere, New York.

Macdonald, P.P., Lee, C.B., 2004. Use of thoria–urania fuels in PWRs: A general review of a NERI project to assess feasible core design, economics, fabrication methods, in pile thermal/mechanical behavior, and waste form characteristics. Nuclear Technology 147, 1–7.

March-Leuba, J., 1986. A reduced-order model of boiling water reactor linear dynamics. Nuclear Technology 75, 15–22.

March-Leuba, J., 1990. LAPUR benchmark against in-phase and out-of-phase stability test. NUREG/CR-5605, ORNL/TM-11621.

March-Leuba, J., Blakeman, E.D., 1991. A mechanism for out-of-phase power instabilities in boiling water reactors. Nuclear Science and Engineering 107, 173–179.

March-Leuba, J., Rey, J.M., 1993. Coupled thermal–hydraulic neutronic stabilities, in boiling water reactor a review of the state of the art. Nuclear Engineering and Design 145, 97–111.

NEA, 1997. State of the art report on boiling water reactor stability (SOR on BWRS), NEA/CSNI/R (96)13. Nuclear Energy Agency, OECD. Committee on the Safety of Nuclear Installations.

Núñez-Carrera, A., François, J.L., Espinosa-Paredes, G., 2004. Comparison between HELIOS critical calculations and PWR thorium cell burnup benchmark. Annals of Nuclear Energy 31, 713–722.

Núñez-Carrera, A., Francois, J.L., Martin-del-Campo, C., Espinosa-Paredes, 2005. Design of a boiling water reactor core based on and integral blanket–seed thorium–uranium concept. Annals of Nuclear Energy 32, 558–571.

Núñez-Carrera, A., Francois, J.L., Martin-del-Campo, C., Espinosa-Paredes, 2008. Feasibility study of a boiling water reactor core based on thorium–uranium fuel concept. Energy Conversion & Management 49, 47–53.

Ronen, Y., 1986. In: Hanbook of Nuclear Reactor Calculations, vol. III. CRC Press, Boca Raton, FL.

Saglam, M., Sapyta, J., Spetz, S., Hassler, L., 2005. Core design and economic analyses of homogeneous thoria–urania fuel in light water reactors. Nuclear Technology 147, 8–19.

Saha, P., Zuber, N., 1974. Point of net vapor generation and vapor void fraction in subcooled boiling. In: Proc. of Fifth Int. Heat Transfer Conf.

Scandpower, 1992a. User manual for CM-PRESTO-91.

Scandpower, 1992b. User manual for TABGEN.

Scandpower, 1992c. User manual for PETRA-91.

Shwageraus, E., Zhao, X., Driscoll, M.J., Hejzlar, P., Kazimi, M.S., Herring, J.S., 2004. Macroheterogeneous thoria–urania fuels for pressurized water reactor. Nuclear Technology 147, 20–36.

Studsvik Scandpower, 1998. HELIOS 1.5 methods.

Todosow, E., Galperin, A., Herring, S., Kazimi, M., Downar, T., Morozov, A., 2005. Use of thorium in light water reactors. Nuclear Technology 151, 168–176.

Verdu, G., Ginestar, D., Muñoz-Cobo, J.L., Navarro, J., Palomo, M.J., Lansaker, P., Conde, J.M., Recio, M., Sartori, E., 2001. FORSMARK 1 & 2 boiling water reactor stability benchmark, Time series analysis method for oscillations during BWR operation. Final report NEA/NSC/DOC(2001)2. Nuclear Energy Agency, OECD.

Wulff, W., Cheng, H.S., Lekach, S.V., Mallen, A.N., 1984. The BWR plant analyzer, NUREG/CR-3943, BNL-NUREG-51812.

Zuber, N., Findlay, J.A., 1965. Average volumetric concentration in two-phase flow systems. Journal of Heat Transfer 87, 453–468.